# Development of an instrumented and automated flash sintering setup for enhanced process monitoring and parameter control

João V. Campos[1]; Isabela R. Lavagnini[1]; Rafael V. de Sousa[1]*; Julieta A. Ferreira[1]; Eliria M. J. A. Pallone[1].
[1]Departamento de Engenharia de Biossistemas, Universidade de São Paulo, USP
Av. Duque de Caxias Norte, 225, Pirassununga-SP, Brasil.

**Abstract**

Heterogeneous grain size distributions in the microstructure of samples sintered by flash sintering are a recurring problem. Herein, we present the construction, instrumentation, and automation of a furnace for flash sintering with refined control of the process parameters, especially the electric current density, to reduce the grain size heterogeneity of sintered materials. A conventional tubular furnace was adapted and automated with supervisory software with a fast response (60 ms). The real-time control of the equipment enabled the development of a Multi-Step Flash Sintering (MSFS) process. This technique involves varying the maximum current density at the onset of the abrupt shrinkage of the sample during the flash phenomenon, smoothing the shrinkage curve, and allowing its control in real time. Tetragonal stabilised zirconia was sintered in this equipment by both flash sintering and MSFS. Preliminary results of this study were promising in terms of density control and improvement of grain size homogeneity.

**Keywords**: furnace, zirconia, 3YSZ, field-assisted sintering technique.

## Introduction

Flash sintering (FS) was first presented by Cologna, Rashkova, and Raj (2010)[1] and consists in applying an electric field to the sample concomitant with the increase in temperature of the furnace during sintering. The electrical and ionic conductivity of materials with negative temperature coefficients (NTC) are proportional to the temperature. Thus, at a given temperature, an electric current is induced in the sample. The electric current heats the sample abruptly, causing its shrinkage in few seconds, and consequently its densification with low grain growth.

The first material subjected to FS was 3YSZ[1]; it was densified in a few seconds at a temperature of 850 °C and under an applied electric field of 120 V/cm. Such temperature and time are significantly lower than the conventional sintering temperature and time (about 1500 °C for 2 h). Since this pioneering work, several studies have applied the FS technique to other materials, for example, 8YSZ[2], Co2MnO4[3], Al2O3[4], SiC[5], TiO2[6], and ZnO[7]. When compared to other sintering techniques, FS stands out for its ultrafast sample densification and lower temperatures and energy consumption[8]. In addition, due to the rapid densification, there is no time for grain growth, and as a consequence, the materials sintered by FS have a refined microstructure[9].

Current studies aim to unravel the mechanism and optimise the parameters of the FS process and, consequently, the microstructure of the sintered ceramic material. In addition, the need for standard models of FS equipment is highlighted[10]. Research groups studying this technique have developed or adapted furnaces to apply an electric field in situ during the heating of the samples. Dancer (2016)[10] classified three types of FS furnace models. The first one was initially presented by

Cologna, Rashkova, and Raj (2010)[1], who added a thermographic camera to the tubular furnace to measure the shrinkage and temperature of the sample. In this equipment, the sample is suspended by platinum wires that are also used as electrodes for the application of the electric field. The second model was initially proposed by Caliman et al. (2016)[11] and is an adaptation of a dilatometer, with the sample positioned between two electrodes in the form of a disc. These electrodes rest mechanically on two rods. A small load is applied to the movable upper rod to maintain electrical contact between the electrode and the sample, and a displacement sensor is used to measure the shrinkage[11]. The third model, proposed by Zapata-Solvas et al. (2015)[12], is an adaptation of a commercial Spark Plasma Sintering (SPS) furnace. In this model, the traditional SPS graphite mould is not used, and the sample should be shaped before insertion. The SPS furnace graphite bars are used as electrodes[12]. Francis and Raj (2013)[13] showed that the current density during FS has a direct influence on the densification. Therefore, it is hypothesised that controlling the current density during the flash phenomenon can control the densification. In addition, Nie et al. (2017)[14] and Charalambous et al. (2018)[15] hypothesised that a refined control of the current density can also influence the size and homogeneity of the grains of the sintered material. Therefore, we propose an adapted, instrumented, and automated tubular furnace assembly for FS, which aims to control the electrical variables in real time during the flash phenomenon. We attempt the programming and control of several levels of current densities with periods of the order of milliseconds during FS to allow the development of a new variation of the technique, herein called Multi-Step Flash Sintering (MSFS).

## Material and methods

The work was carried out in two main stages: (I) the design and construction of the furnace; and (II) the experimental validation of the automated furnace and MSFS technique. The first stage consisted of the following steps: the mechanical adaptation on the design of a conventional furnace structure; the instrumentation and deployment of power electronics; and the construction of a logic controller. The second stage involved the preparation of samples and the sintering experiments to validate the control of the FS process and the possibility of performing MSFS

### Mechanical Adaptation

A vertical tubular furnace, designed to operate at temperatures up to 1700 °C, was adapted as a FS furnace. Figure 1 shows the design of the tubular furnace and its main components. The heating system consists of six molybdenum disilicate (MoSi2) resistors that can reach temperatures of 1800 °C. The muffle of the furnace is octagonal and was assembled from thermal insulation ceramic plates. The furnace is powered by an electric potential of 220 V and has an electric power of 5.5 kW. Figure 1 (a) illustrates the mechanical scheme and the main parts of the furnace, and Figure 1 (b) shows a picture of the adapted FS furnace.

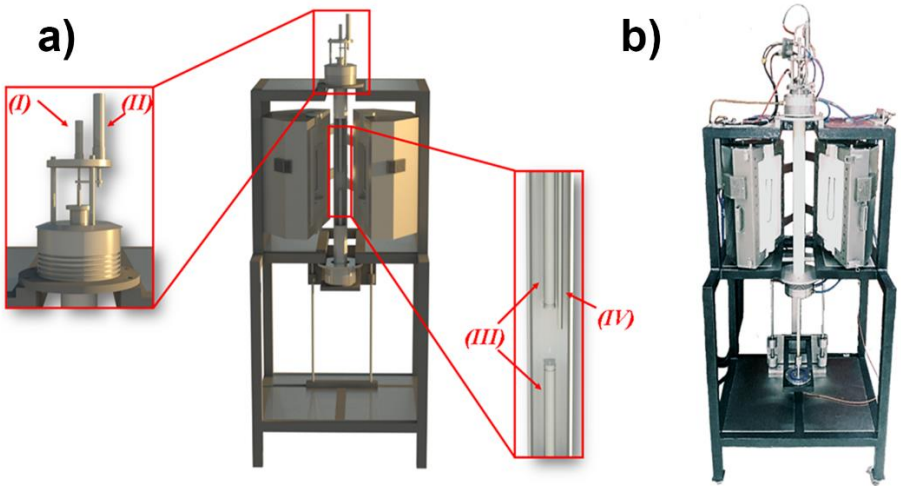


**Figure 1** Illustration of the tubular furnace adapted to perform FS: a) representation highlighting the main elements (i) pneumatic cylinder; (ii) LVDT displacement sensor; (iii) mechanical support rods; (iv) "S" type thermocouple and b) picture of the FS adapted furnace.

An alumina tube (50 mm internal diameter, 54 mm external diameter, and 830 mm long) is placed in the middle of the muffle (Figure 1 (a)). The samples are placed inside the tube between two platinum electrodes in the form of discs that are 3-mm thick at a height corresponding to the centre of the muffle. These electrodes are attached to alumina rods (13 mm diameter and 250 mm long) that were also used as a mechanical support (Figure 1 (a) – (III)). An electric elevator is used to move the bottom rod and place the sample at the centre of the alumina tube. The upper rod is movable and rests on a stainless-steel cap that is laid above the alumina tube. The upper rod is also connected to a double-stage pneumatic cylinder with a maximum pressure of 10 bar, which is used to apply the mechanical load, and to a displacement sensor used to measure the sample shrinkage in situ (Figure 1 (a) – (I) and (II)). The electrodes are connected to the power supply by platinum wires.

Instrumentation and Power Electronics

An electrical panel was installed to power the sensors and electrical actuators and support the power system and logic control. The main constituent elements of this panel are:

- A programmable logic controller (PLC), DVP20SX211T, Delta;
- A human-machine interface screen (HMI), DOPB07E515, Delta;
- Two proportional integral derivative (PID)-type temperature controllers (CT-1 and CT-2);
- A power control unit (PwC);
- A thyristor for power output controlled by the PwC;
- A digital pressure regulating valve (pneumatic circuit);
- Seven auxiliary relays controlled by the PLC.

The valves and pneumatic cylinder constitute the pneumatic circuit and allow the load application on the sample during the FS process. This pneumatic circuit is controlled by auxiliary relays connected to the PLC. In addition, a 10-µm precision LVDT displacement sensor (LD630-10, Omega) is attached to the movable part of the pneumatic cylinder to measure the sample shrinkage during the FS process (Figure 1 (a) - II). The sensor is powered by the electrical panel and is connected directly to the PLC.

For the temperature measurement, an "S" type thermocouple measuring temperatures up to 1700 °C collects the temperature data close to the MoSi2 resistors. In addition, there is a second thermocouple located next to the upper rod inside the tube (Figure 1 (a) – (IV)). This second thermocouple was introduced to measure the temperature variation close to the sample (3 mm distance) during FS. These sensors are directly connected to the temperature controller, which is connected to the PLC. The temperature control of the furnace is performed in several steps. First, the CT-1 receives the value of temperature of the furnace measured

by the thermocouple located near the resistors. The PwC compares the expected temperature determined from a proportional integrative derivative (PID) control routine and the actual temperature to control the thyristor. Then the thyristor controls the supply of electrical current to the resistors and thus the electrical power. A programmable electrical source (751iX series II, California Instruments) with a maximum power of 750 W is used to generate an electric field and control the current during FS. This source can operate as a current and voltage control with variable parameters such as the voltage, current, mode (alternating, continuous, and hybrid), waveform, and frequency. This source has a voltmeter and ammeter connected internally to measure the voltage and electric current that is effectively consumed during FS.

An elevator is used to place the sample in the centre of the muffle. This elevator is driven by an electric motor of direct current (DC). Limit switches are located on the bottom flange and at the base of the frame. Thus, when the elevator reaches its final stroke, the motor is switched off automatically, both for ascent and for descent. This system is controlled via the computer and HMI control panel.

Logic control

Three different control softwares were developed, one for the PLC, one for the HMI, and the third for a desktop computer (PC). The PLC logic program was implemented in the Ladder language and programming environment provided by the PLC manufacturer (Delta). For control via HMI, we developed a program in the language and programming environment of the manufacturer (DOPSoft V2.00.06), which is similar to the C++ programming language. We also developed a supervisory software in the language and programming environment LabVIEW 2013 (National Instruments). This supervisory software enables the monitoring and control of the

parameters of the furnace and power source from a PC. In addition, it allows the visualisation of these parameters in real time in the form of graphs and collects all variables data in the automated system during the FS process. To establish communication between the sensors and actuators, the PLC, the HMI, and the supervisory software (located in the PC), a communication hierarchy was created. Figure 2 shows the communication network topology and information flow between the system components, showing the communication channels and protocols used in each subnet.

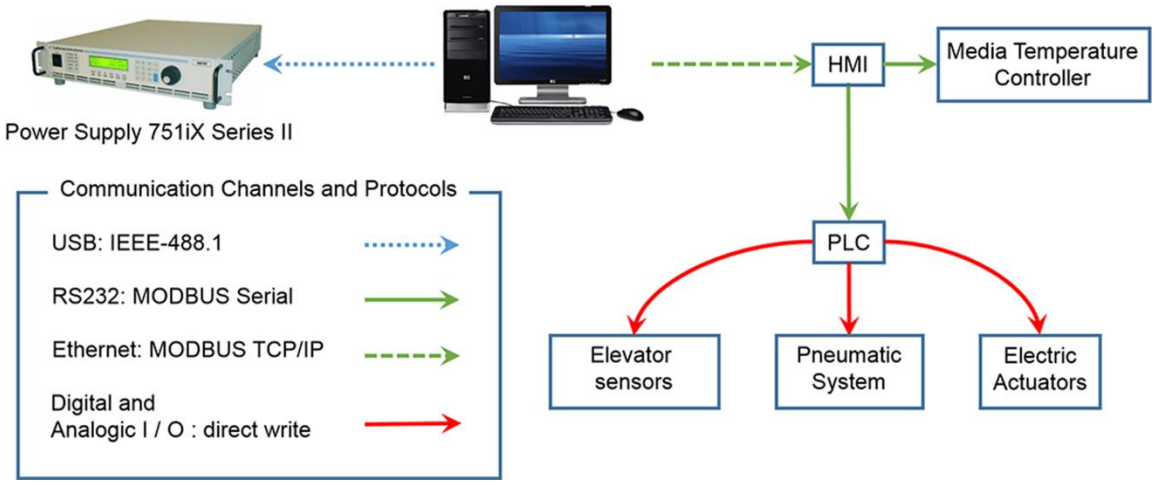


**Figure 2** Communication network topology and information flow integrating the FS process automation elements.

Communication between the PLC, sensors, and system actuators is established directly from the digital and analogue inputs and outputs (Figure 2). Communication between the PLC and the HMI is established from a standard MODBUS ASCII subnet (via RS232 serial port). In turn, communication between the supervisory program (located on a PC) and the HMI is established from a standard MODBUS TCP/IP subnet (via an Ethernet port). In addition, the supervisory program communicates with the programmable electrical source via the USB-RS232C conversion interface.

The communication protocol used in this case was ANSI/IEEE Std. 488.1 (1987).

The supervisory software developed in LabVIEW allows the configuration of the following FS parameters: furnace heating rate and temperature thresholds; pneumatic cylinder pressure; elevator position; electric field and current density magnitude; AC or DC mode; frequency and waveform of the AC electric current or voltage. In addition, it is possible to monitor and save the collected data in real time (60 ms acquisition rate): the temperatures read by the two thermocouples (near the sample and near the furnace resistors), the mechanical pressure applied in the pneumatic cylinder, the electric field applied, the linear shrinkage, and the electric current density. In addition to the described functionalities of the supervisory software, we added a routine that allows MSFS. Therefore, we defined parameters, such as the number of electric current density stages, their occurrence times in milliseconds, and current density magnitude for each one of these stages. The routine then varied these parameters during the flash phenomenon and enabled the creation of ramps to increase and decrease the electric current on the sample. This variation of the FS technique is referred here as MSFS.

Sample processing and sintering

To test the reproducibility of the equipment as well as its ability to perform MSFS, samples of 3YSZ were prepared. The Tosoh commercial powder TZ-3Y-E was used (mean particle size of 40 nm and specific surface area of 16 ± 3 $m^2/g$). This powder was milled in an alcoholic suspension containing 0.5 wt% 4-aminobenzoic acid (PABA; Vetec Ltd.) and 0.5 wt% oleic acid (Vetec Ltd.) for 24 h in a ball mill to reduce the agglomerate size[16]. The resulting suspension was dried under a continuous stream of air until all traces of alcohol were removed. The resulting powder was

run through an 80-mesh sieve (Tyler scale). The shaping of the samples in a cylinder (6 mm in diameter and 5 mm in height) was performed in a uniaxial press at 70 MPa followed by isostatic pressing at 200 MPa (AIP CP360 equipment). The cylindrical samples were calcined for 60 min at a heating rate of 5 °C/min and a temperature of 800 °C in a conventional furnace (EDG3P-S, EDG). To verify the reproducibility of the equipment, several FS experiments were performed by varying the electric current density (60, 80, and 100 mA/mm²), the electric field (90, 120, and 180 V/cm), and the frequency (DC or AC at 50 Hz and 1000 Hz). These values were based on studies found in the literature[1,13,17]. Three MSFS experiments were also performed; one by slowly varying the current density in four steps at 20 s/step (33, 66, 99, 200 mA/mm²); and another two by rapidly varying the current density in 120 steps at 500 ms/step from 0.1 mA/mm² to 100 mA/mm² for the ascent ramp and from 100 mA/mm² to 0.1 mA/mm² for the descent ramp. In all FS and MSFS experiments, the adapted tubular furnace was heated at a rate of 20 °C/min, and the electric field was applied at the beginning of the heating process. In the FS experiments, the field was turned off after 60 s of the occurrence of the flash phenomenon (time at which the current density reaches a pre-defined maximum value). In the MSFS experiments, the field was turned off after the defined thresholds were reached. The mechanical pressure was 2 bar. At the onset of the flash phenomenon, the source starts to operate in the electric current control mode and does not allowing the current to exceed the pre-set value; thus, it no longer controls the electric field. The microstructural analysis of the fracture surface of the samples sintered by FS and MSFS was performed using a scanning electron microscope, Philips FEG XL-30.

## Results and discussion

The results were divided into conventional FS and MSFS, aiming at evidencing the variables that were controlled during the process and their influence on the microstructure of the sintered material.

Conventional flash sintering

Figures 3 (a) and (b) show the electric field (E), current density (J), specific power density (P), and specific shrinkage (dL/Lo) following FS with AC (1000 Hz) and DC under an electric field of 120 V/cm and a current density of 100 mA/mm². As expected, the curves closely resemble the results found in the literature[1,17,18], especially the curves obtained from the samples sintered using AC (Figure 3 (a)). At the instant of the "flash", the source starts to operate in the electric current control mode. Thus, the electric field (E) decreases as the current density (J) increases, until equilibrium is reached. Then, the sample shrinks rapidly (linear shrinkage represented as dL/Lo). The curves obtained under the other conventional FS conditions were quite similar to those presented in Figures 3 (a) and (b).

Region (I) of Figure 3 (a) and region (II) of Figure 3 (b) highlight the power peaks occurring during the apex of the flash phenomenon (at which point almost all sample shrinkage occurs). Some authors have suggested that this power peak favours grain growth and that the control of this peak could lead to improvements in the microstructure of the sintered material[14,15].

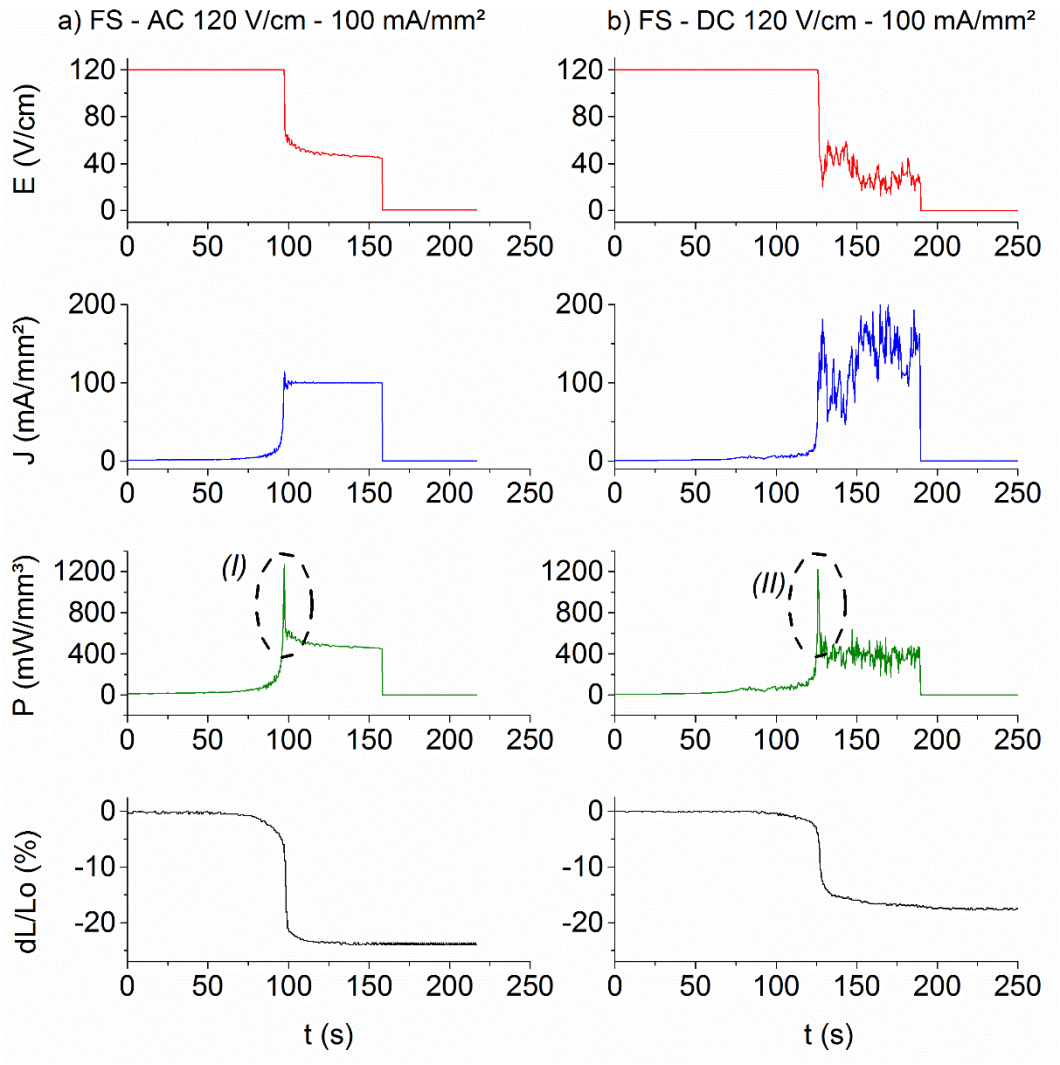


**Figure 3** Electrical field curves (E), current density (J), specific power (P), and specific shrinkage (dL/Lo) of the sample sintered by FS with (a) AC 1000 Hz at 120 V/cm and 100 mA/mm2 and (b) DC at 120 V/cm and 100 mA/mm2. The highlighted region (i) and (ii) correspond to the observation of the electrical power peak.

When comparing the linear shrinkage curves (dL/Lo), the samples sintered with DC underwent lower linear shrinkage than those sintered with AC, resulting in a lower bulk density.

Table 1 shows the bulk densities of the samples for each of the FS experiments. The data were organised according to the temperature (from

lowest to highest value) of the occurrence of the flash phenomenon (abrupt densification) for each the electric field variation, current density, and frequency. In general, the flash phenomenon of the samples under higher electric fields occurred at lower temperatures. This result was expected because the electrical conductivity required to induce an electric current in the sample should be lower under electric fields of greater magnitude. Thus, for NTC-type samples, the higher the electric field, the lower the temperature required for the occurrence of the flash phenomenon[13].

| Furnace Temperature (°C) | E (V/cm) | J (mA/mm²) | ν (Hz) | Bulk Density (%) |
|---|---|---|---|---|
| 794 | 180 | 60 | CC | 73,11 ± 0,69 |
| 795 | 180 | 60 | 1000 | 91,20 ± 0,17 |
| 796 | 180 | 100 | CC | 81,90 ± 0,91 |
| 803 | 180 | 80 | CC | 77,63 ± 0,72 |
| 817 | 180 | 60 | 50 | 88,03 ± 0,32 |
| 822 | 180 | 80 | 1000 | 92,66 ± 1,07 |
| 828 | 180 | 80 | 50 | 90,04 ± 1,18 |
| 836 | 180 | 100 | 50 | 91,80 ± 0,82 |
| 842 | 180 | 100 | 1000 | 92,93 ± 1,13 |
| 857 | 120 | 100 | 50 | 91,16 ± 0,66 |
| 877 | 120 | 100 | CC | 81,77 ± 0,32 |
| 889 | 120 | 80 | 1000 | 93,58 ± 1,14 |
| 889 | 120 | 60 | 50 | 89,00 ± 0,81 |
| 891 | 120 | 80 | CC | 79,14 ± 0,99 |
| 892 | 120 | 60 | CC | 77,70 ± 0,39 |
| 899 | 120 | 80 | 50 | 93,13 ± 0,54 |
| 903 | 90 | 60 | 1000 | 94,91 ± 0,46 |
| 914 | 90 | 100 | 50 | 91,96 ± 0,71 |
| 918 | 90 | 100 | 1000 | 95,10 ± 0,66 |
| 918 | 90 | 80 | 1000 | 96,69 ± 0,38 |
| 918 | 120 | 100 | 1000 | 93,21 ± 0,47 |
| 929 | 90 | 60 | CC | 80,20 ± 0,59 |
| 933 | 120 | 60 | 1000 | 90,94 ± 0,92 |
| 937 | 90 | 80 | 50 | 93,62 ± 0,16 |
| 939 | 90 | 80 | CC | 81,77 ± 0,58 |
| 940 | 90 | 100 | CC | 85,23 ± 0,32 |
| 943 | 90 | 60 | 50 | 90,71 ± 0,92 |

**Table 1** Onset temperature of FS for the different electric fields, current densities, frequencies and bulk densities of the corresponding samples.

According to Table 1, the bulk densities of the samples sintered with DC are lower than those sintered with AC due to the heterogeneity in sintering with a DC. The side of the sample in contact with the cathode (positive electrode) underwent considerably greater shrinkage compared to the side in contact with the anode (negative electrode). Figures 4 (a), (b), and (c) illustrate the samples before sintering and sintered in with AC and DC, respectively. A heterogeneous shrinkage can be observed in the sample sintered with DC (Figure 1 (c)), which led the sample to exhibit a conical shape.

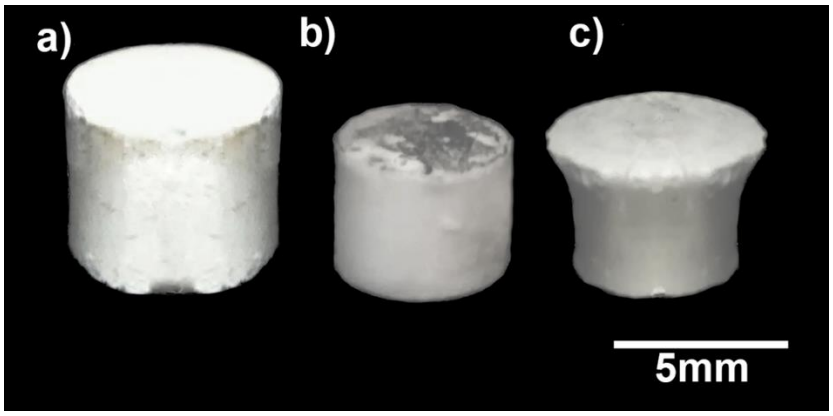


**Figure 4** Samples of 3YSZ (a) before sintering; (b) sintered by FS with AC of 1000 Hz; and (c) sintered by FS with DC with J= 60 mA/mm2 and E = 90 V/cm.

In addition to the shrinkage heterogeneity, the DC samples exhibited a different behaviour with respect to the oscillation compared to samples sintered with AC, as shown in Figure 3. Figure 5 (a) and (b) show the changes in the electric field during the flash phenomenon with different current densities and with DC or AC. The electric field curves exhibit little oscillation during FS with AC (Figure 5 (a)) compared to FS with DC for current densities higher than 60 mA/mm² (Figure 5 (b)). This behaviour shows that the control of the electric current by the source during the flash phenomenon is in higher demand when using DC than AC for

current densities higher than 60 mA/mm². An explanation for this behaviour requires further scientific investigation, but it can be affirmed that the electric source controls the current in the DC mode, although with possible feedback error in the upper control mesh.

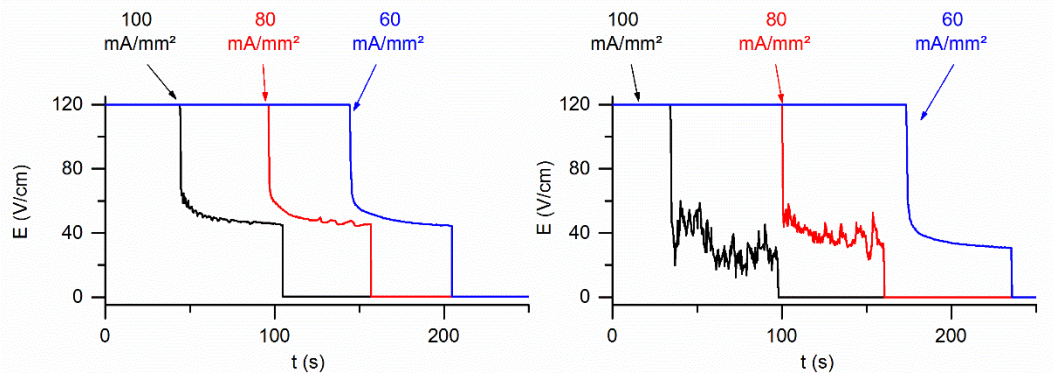


**Figure 5** Comparison of the electric field curves under a current density of 100, 80, and 60 mA/mm2 by time during the flash phenomenon using (a) AC and (b) DC.

Todd et al. (2015)[19] varied the maximum current during FS and observed that the higher the electric current limit in the source, the more chaotic the electric field curve. According to the authors, the oscillations in the electric field occur due to the increase in the temperature of the sample because of the increase in the current density (due to the Joule effect). Thus, because 3YSZ is an NTC material, its conductivity increases with the temperature, producing a chaotic effect that substantially hinders the control of the electric source. Therefore, the higher the applied current, the greater the conductivity variation and the more difficult the parameter control. However, the explanation given by Todd et al. (2015)[19] is only valid in the DC mode, and therefore does not address why the absence of this phenomenon in the samples sintered with AC.

A possibility not yet explored in the literature is that the chaotic variation of the electric field in DC and the high current densities arise because of a lack of molecular oxygen in the vicinity of the negative electrode. According to Caliman et al. (2016)[11], a reversible chemical reaction occurs between the atmosphere near the electrodes and the electrode/sample interface. In this reaction, molecular oxygen is ionised by the induced ionic current and transports charges through the sample. At a high electric current density, the electrochemical reaction may require more molecular oxygen than what is present in the control volume. Thus, in the DC mode with high current densities, a lack of molecular oxygen can occur, which can generate the chaotic effect shown in Figure 5 (b). This would not occur in the AC mode because the reverse reaction occurs at the same electrode at a frequency of 50 and 1000 Hz, which does not allow molecular oxygen to be lacking in the control volume (Figure 5 (a)).

Figure 6 shows micrographs of the fracture surface in different regions of the samples sintered by FS in the AC mode at 1000 Hz under and electric field of 120 V/cm and a maximum current density of 100 mA/mm² (RMS). It is evident that the material presents a larger grain size at the centre, i.e., region (II), that in the other regions closer to the surface in contact with the electrode, i.e., regions (I) and (III). Carvalho et al. (2018)[20] attributed this behaviour to non-uniformity in the sample density, which is caused by the pressure gradients generated during the shaping. Non-uniformity in the sample density results in a conductivity gradient. In regions with higher resistivity, the Joule effect is enhanced by heating and provides more energy for grain growth. In FS models based on Joule effect heating, it is considered that the supplied power is dissipated on the surface of the sample by radiation

via the light emitted during the flash phenomenon[19,21]. Thus, the surface dissipates heat more easily than the centre (which dissipates heat only by conduction), which generates a temperature gradient in the sample. To avoid this temperature gradient, the FS could be operated under a quasi-adiabatic regime, i.e., in a short period of time[22]. Another approach would be the use of thicker samples, which would favour heat exchange by conduction between the centre and the surface, thus increasing the thermal homogeneity.

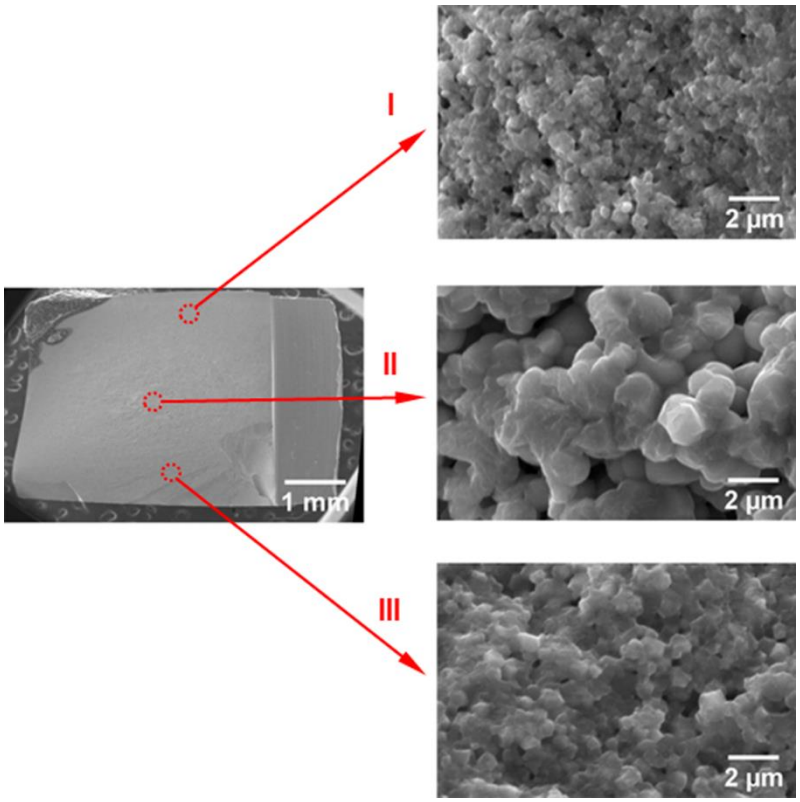


**Figure 6** Micrographs of the fracture surface in three different regions of the sample of 3YSZ sintered by AC: Region I - edge of the sample near the upper electrode; Region II - radial and longitudinal centre; Region III - sample border near the lower electrode.

The heterogeneity of the samples sintered with DC was even greater. In addition, the size distribution differed from that in samples sintered with AC, as the centre did not present a larger grain size. The side

closest to the positive electrode, i.e., region (III) of Figure 7, has a grain size much bigger than the other regions. The behaviour of the DC samples cannot be explained solely by models based on the Joule effect and power dissipation by radiation. Kim et al. (2011)[23] observed this same behaviour in 8YSZ upon measuring the size of the grains near the cathode (+) and the anode (-). Grains close to the cathode were up to 100 times larger than those close to the anode. The authors suggested that this behaviour was caused by a saturation of oxygen vacancies by O-2 ions in the anode region, thus reducing the mobility and consequently the conductivity in this region. Moreover, although there are large grains (in the order of ~12 µm), necks are formed between the grains and their neighbours, suggesting that even before densification, grain growth was favoured in FS.

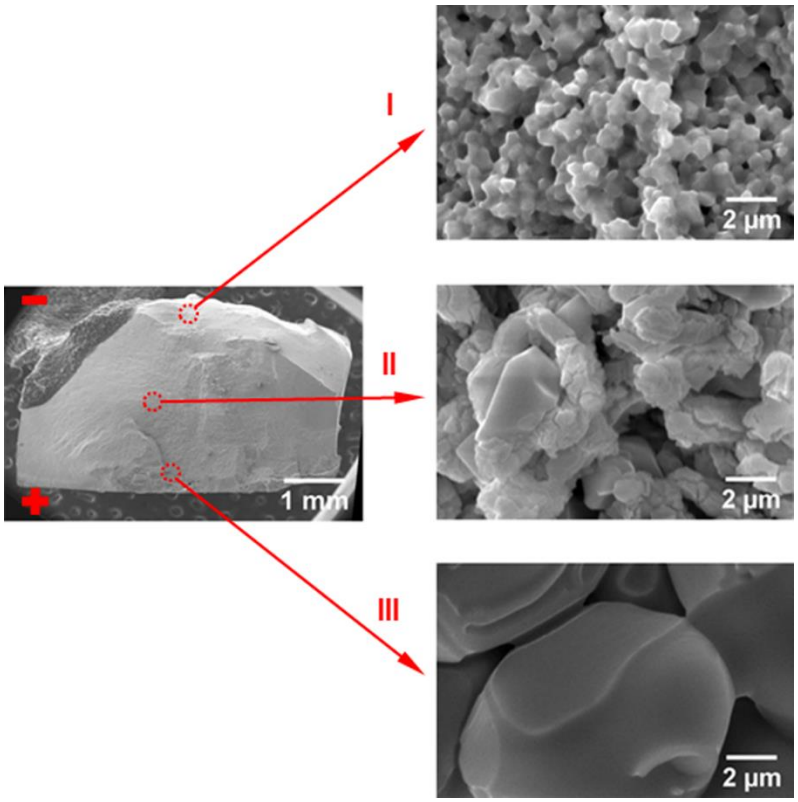


**Figure 7** Micrographs of the fracture surface of 3YSZ sintered with DC under an electric field of 120 V/cm and a current density of 100 mA/mm², where "+" and "-" indicate the positive (cathode) and negative (anode) electrodes. Region I - border near the anode; Region II - radial and longitudinal centre; Region III - edge near the cathode.

In a qualitative analysis of the samples sintered with AC (Figure 6) and DC (Figure 7), it is evident that for the same electric field and current density, samples sintered with AC presented smaller grain size and greater homogeneity than those sintered with DC. A similar observation was made for samples sintered with DC and AC under the other studied conditions.

Multi-step flash sintering – MSFS

The samples sintered by MSFS had bulk densities close to the conventional FS results presented in Table 1. The bulk density for the

samples obtained by MSFS with the ascent ramp, descent ramp, and in four steps was 91.32 ± 0.08%, 90.23 ± 0.12%, and 95.79 ± 0.13%, respectively.

Figure 8 shows the electric field curves, current density, specific power, and specific linear shrinkage of the samples sintered by the MSFS technique. Figure 8 (a) shows the ascent ramp sintering curves, Figure 8 (b) shows the descent ramp sintering curves, and Figure 8 (c) presents the sintering curve obtained in four steps of current density, where each step lasted 20 s.

The experiment with four steps (Figure 8 (c)) is a variation of the Two-Step Flash Sintering (TSFS) process, in which instead of using two steps of descent as proposed by Nie et al. (2017)[14], four ascent steps were created. This experiment was performed to observe the influence of the current density on the linear shrinkage. It should be noted that a linear shrinkage step occurs at each current density step, evidencing the interdependence of these two parameters. In this MSFS variation, a maximum current density of 200 mA/mm² was applied, while in all other FS and MSFS experiments, the maximum current density was 100 mA/mm². This higher current density was probably responsible for the higher densification (95.79 ± 0.13%) of the sintered sample compared to the other samples presented in this work.

The upward and downward curves of the current density could only be acquired upon the instrumentation and automation of the furnace using a supervisory software of fast command (60 ms) that controls the entire system.

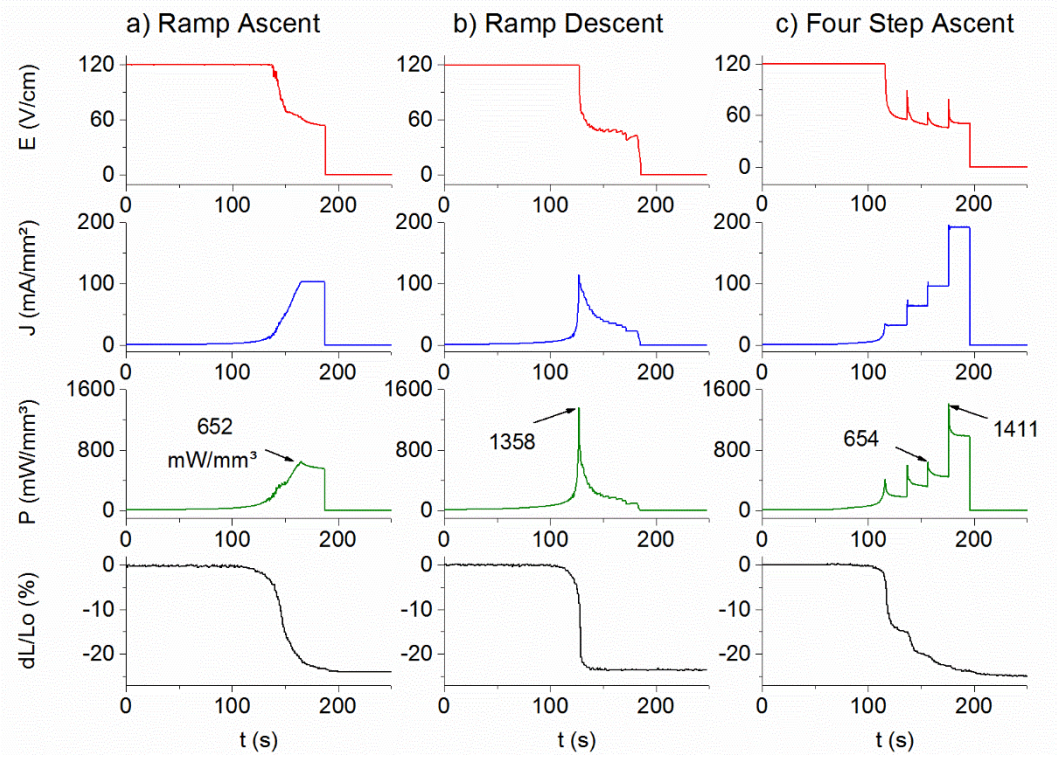


**Figure 8** Electrical field curves (E), current density (J), specific power (P), and specific shrinkage (dL/Lo) of samples sintered by MSFS at 120 V/cm: a) ascent ramp of 0.2 mA/mm² per second; b) descent ramp of 0.2 mA/mm² per second; and c) four current densities 33, 66, 99, and 200 mA/mm² for 20 s each.

The possibility to control the linear shrinkage from the automatic control of the current density, and thus allowing a control of the densification of the material, is highlighted as a positive feature of the MSFS technique. In conventional FS, the shrinkage occurs so abruptly that it becomes impossible to stop sintering prior to maximum densification (for the applied current density). Thus, a technique allowing the control of the final density of the material was established here.

Another positive feature of the MSFS technique is the reduction of the common power peak in the conventional FS technique (Figure 8 (a)). A

recurrent problem in FS is the non-homogeneity of the sample grain sizes[20,22,23], which may be a consequence of the power peaks generated in conventional FS.

Figure 9 shows the microstructure of two different regions of the samples sintered by MSFS with the ascent ramp. Region (I) is close to the surface in contact with the electrode, whereas region (II) is at the longitudinal and radial centre of the sample. There is no grain size heterogeneity in these regions, which indicated that the control of the current density could improve the microstructure of the material.

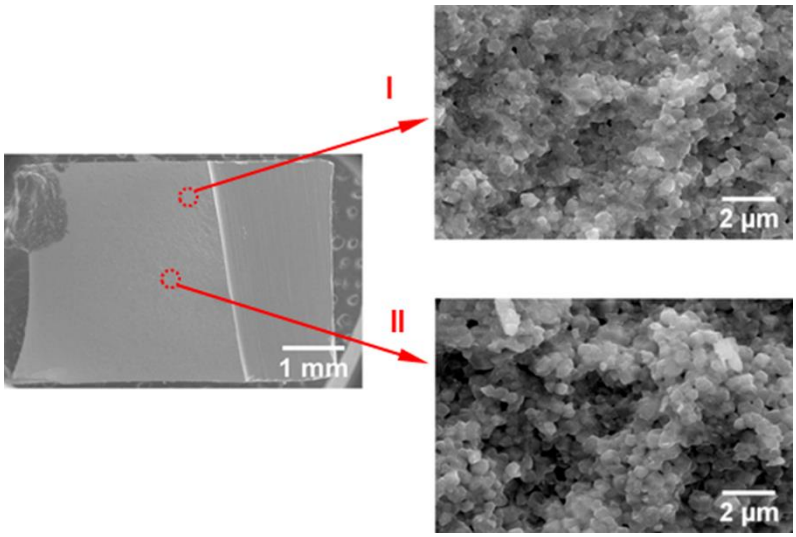


**Figure 9** Micrographs of the fracture surface of 3YSZ sintered by MSFS with the ascent ramp with AC of 1000 Hz with an electric field of 120 V/cm and a maximum current density of 100 mA/mm². Region I - upper border near the electrode; Region II - radial and longitudinal centre.

Figure 10 shows two regions of the microstructure of the sample sintered by MSFS using the descent ramp. Region (I) is close to the surface in contact with the electrode, while region (II) lies in the longitudinal and radial centre of the sample. Note that even with the power peak as in the conventional FS (Figure 8), the samples obtained by this method did not show heterogeneity in grain size. Further detailed

studies of the technique are needed to explain the uniformity of microstructures obtained by MSFS.

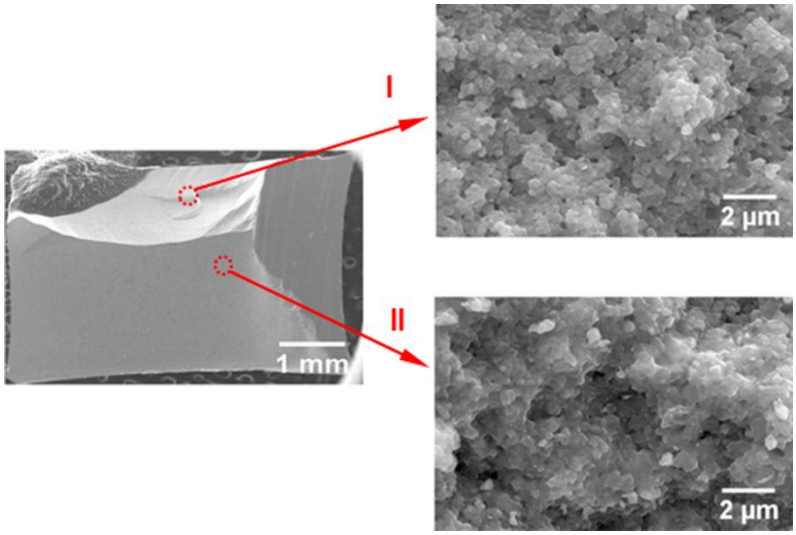


**Figure 10** Micrographs of the fracture surface of 3YSZ sintered by MSFS with the descent ramp with AC of 1000 Hz with an electric field of 120 V/cm and a maximum current density of 100 mA/mm². Region I - upper border near the electrode; Region II - radial and longitudinal centre.

In a qualitative comparison between the samples sintered by MSFS with the ascent (Figure 9) and descent (Figure 10) ramps and those sintered by conventional FS (Figure 6), a much lower grain size is observed in the MSFS samples.

The proposed automated system produced positive results from the control of the variables associated with the flash phenomenon during the sintering process. The results obtained by the MSFS technique, although preliminary, proved to be distinct from those obtained by conventional FS. As shown in Figure 8, the current density curves were quite different from the traditional ones (Figure 3). In addition, a variation of the TSFS[14] was performed, where two more steps of current density were included. These results attest, albeit preliminarily, to some assumptions in the literature that the control of the current density curve could

provide significant improvements in the microstructure of materials sintered by FS[14,15]. Finally, the results indicated that detailed investigations of the variation of the parameters of the up and down ramps of MSFS are necessary for a better understanding and refinement of this new variation of the FS technique.

**Conclusions**

The tubular furnace was adapted and automated to perform FS, and the obtained results were validated by comparison with the literature.

The current density could be controlled in real time with the built-in supervisory software, allowing the application of a variation in the FS technique referred here as MSFS. In MSFS, the power peaks that favour grain growth could be avoided. Preliminary microstructural analyses showed homogeneity in grain size and growth both at the centre and on the surfaces of the materials sintered by MSFS

**Acknowledgements**

Funding: This work was supported by the São Paulo State Research Support Foundation (FAPESP) [2015/07319-8, and 2018/04331-5], and the Coordination for the Improvement of Higher Education Personnel - Brazil (CAPES) [001].

**References**

[1] M. Cologna, B. Rashkova, R. Raj, Flash sintering of nanograin zirconia in < 5 s at 850°C, J. Am. Ceram. Soc. 93 (2010) 3556–3559. doi:10.1111/j.1551- 2916.2010.04089.x.

[2] M. Cologna, A.L.G. Prette, R. Raj, Flash-sintering of cubic yttria-stabilized zirconia at 750°C for possible use in SOFC manufacturing, J. Am. Ceram. Soc. 94 (2011) 316– 319. doi:10.1111/j.1551-2916.2010.04267.x.

[3] A.L.G. Prette, M. Cologna, V. Sglavo, R. Raj, Flash-sintering of Co2MnO4 spinel for solid oxide fuel cell applications, J. Power Sources. 196 (2011) 2061–2065. doi:10.1016/j.jpowsour.2010.10.036.

[4] M. Cologna, J.S.C. Francis, R. Raj, Field assisted and flash sintering of alumina and its relationship to conductivity and MgO-doping, J. Eur. Ceram. Soc. 31 (2011) 2827– 2837. doi:10.1016/j.jeurceramsoc.2011.07.004.

[5] E. Zapata-Solvas, S. Bonilla, P.R. Wilshaw, R.I. Todd, Preliminary investigation of flash sintering of SiC, J. Eur. Ceram. Soc. 33 (2013) 2811–2816. doi:10.1016/j.jeurceramsoc.2013.04.023.

[6] S.K. Jha, R. Raj, The Effect of Electric Field on Sintering and Electrical Conductivity of Titania, J. Am. Ceram. Soc. 97 (2014) 527–534. doi:10.1111/jace.12682.

[7] C. Schmerbauch, J. Gonzalez-julian, R. Roder, C. Ronning, O. Guillon, Flash Sintering of Nanocrystalline Zinc Oxide and its Influence on Microstructure and Defect Formation, J. Am. Ceram. Soc. 97 (2014) 1728–1735. doi:10.1111/jace.12972.

[8] D. Sohrabi, B. Heidary, M. Lanagan, C.A. Randall, Contrasting energy efficiency in various ceramic sintering processes, J. Eur. Ceram. Soc. 38 (2018) 1018–1029. doi:10.1016/j.jeurceramsoc.2017.10.015.

[9] J. M'Peko, J.S.C. Francis, R. Raj, Impedance spectroscopy and dielectric properties of flash versus conventionally sintered yttria-doped zirconia electroceramics viewed at the microstructural level, J. Am. Ceram. Soc. 96 (2013) 3760–3767. doi:10.1111/jace.12567.

[10] C.E.J. Dancer, Flash sintering of ceramic materials, Mater. Res. Express. 3 (2016) 1– 25. doi:http://dx.doi.org/10.1088/2053-1591/3/10/102001.

[11] B.L. Caliman, R. Bouchet, D. Gouvea, P. Soudant, M.C. Steil, Flash sintering of ionic conductors : The need of a reversible electrochemical

reaction, J. Eur. Ceram. Soc. 36 (2016) 1253–1260. doi:10.1016/j.jeurceramsoc.2015.12.005.

[12] E. Zapata-Solvas, D. Gómes-García, A. Domínguez-Rodríguez, R.I. Todd, Ultra-fast and energy-efficient sintering of ceramics by electric current concentration, Sci. Rep. 5 (2015) 8513. doi:10.1038/srep08513.

[13] J.S.C. Francis, R. Raj, Influence of the field and the current limit on flash sintering at isothermal furnace temperatures, J. Am. Ceram. Soc. 96 (2013). doi:10.1111/jace.12472.

[14] J. Nie, Y. Zhang, J.M. Chan, S. Jiang, R. Huang, J. Luo, Two-step flash sintering of ZnO : Fast densification with suppressed grain growth, Scr. Mater. 141 (2017) 6–9. doi:10.1016/j.scriptamat.2017.07.015.

[15] H. Charalambous, S. Krishn, R.T. Lay, A. Cabales, J. Okasinski, T. Tsakalakos, Investigation of temperature approximation methods during flash sintering of ZnO, Ceram. Int. 44 (2018) 6162–6169. doi:10.1016/j.ceramint.2017.12.250.

[16] A. Scoton, A. Chinelatto, A. Luiz, C. Lago, J. Adriana, E. M. J. A. Pallone, Effect of sintering curves on the microstructure of alumina – zirconia nanocomposites, Ceram. Int. 40 (2014) 14669–14676. doi:10.1016/j.ceramint.2014.06.055.

[17] J.S.C. Francis, R. Raj, Flash-sinterforging of nanograin zirconia: Field assisted sintering and superplasticity, J. Am. Ceram. Soc. 95 (2012) 138–146. doi:10.1111/j.1551-2916.2011.04855.x.

[18] R. Muccillo, E.N.S. Muccillo, An experimental setup for shrinkage evaluation during electric field-assisted flash sintering: Application to yttria-stabilized zirconia, J. Eur. Ceram. Soc. 33 (2013) 515–520. doi:10.1016/j.jeurceramsoc.2012.09.020.

[19] R.I. Todd, R.S. Bonilla, T. Sneddon, P.R. Wilshaw, Electrical characteristics of flash sintering : thermal runaway of Joule heating, J.

Eur. Ceram. Soc. 35 (2015) 1865–1877. doi:10.1016/j.jeurceramsoc.2014.12.022.

[20] S.G.M. Carvalho, E.N.S. Muccillo, R. Muccillo, Electrical Behavior and Microstructural Features of Electric Field-Assisted and Conventionally Sintered, Ceramics. 1 (2018) 1–10. doi:10.3390/ceramics1010002.

[21] I.J. Hewitt, A.A. Lacey, R.I. Todd, A Mathematical Model for Flash Sintering, Math. Model. Nat. Phenom. (2015) 1–16. doi:10.1051/mmnp/201510607.

[22] M.C. Steil, D. Marinha, Y. Aman, J.R.C. Gomes, M. Kleitz, From conventional ac flash-sintering of YSZ to hyper-flash and double flash, J. Eur. Ceram. Soc. 33 (2013). doi:10.1016/j.jeurceramsoc.2013.03.019.

[23] S. Kim, S.G. Kim, J. Jung, S.L. Kang, I. Chen, Enhanced grain boundary mobility in yttria-stabilized cubic zirconia under an electric current, J. Am. Ceram. Soc. 94 (2011) 4231–4238. doi:10.1111/j.1551-2916.2011.04800.x.